



Published in final edited form as:

*Biomacromolecules*. 2012 October 8; 13(10): 3395–3400. doi:10.1021/bm301155w.

## Parallel lipoplex folding pathways revealed using magnetic tweezers

Zhiqiang Sun, Elena B. Tikhonova, Helen I. Zgurskaya, and Valentin V. Rybenkov\*

Department of Chemistry and Biochemistry, University of Oklahoma, 101 Stephenson Parkway, Norman, OK 73019, USA

### Abstract

Lipid-coated DNA nanoparticles (lipoplexes) are a powerful gene delivery tool with promising therapeutic applications. The mechanism of lipoplex assembly remains poorly understood. We explored DNA packing by a cationic lipid DSTAP (distearoyl trimethylammonium-propane) using magnetic tweezers. DSTAP-induced DNA condensation occurred as a series of bursts with the mean step size of 60 nm to 80 nm. The pause time preceding the steps could be approximated as a bimodal distribution, which reveals at least two distinct condensation pathways. The rapidly condensed DNA was more resilient to force-induced decondensation. The proportion of the stable, fast-formed complexes decreased at high salt concentrations. A similar trend was observed in bulk experiments. Lipoplexes assembled at low salt concentration more efficiently shielded DNA from fluorescent dyes and DNase even after transfer to the high salt conditions. These data reveal that lipoplex folding occurs via two parallel pathways even at the single molecule level. The progress through the two pathways can be monitored in real time using single DNA manipulations. The relative efficiency of the two pathways can be varied by external conditions.

### Keywords

lipoplex; cationic lipids; gene delivery; magnetic tweezers; single molecule methods; DNA packing

### Introduction

Lipid-coated DNA nanoparticles (lipoplexes) are widely regarded as a potentially powerful tool for DNA delivery in various clinical and research applications<sup>1–3</sup>. In this approach, cationic liposomes condense DNA into a particle that protects DNA from enzymatic degradation and delivers it into the cells. A major bottleneck in the efficient design of such vectors is the lack of clear understanding how DNA is packed by the lipids<sup>4</sup>.

Significant efforts focused on characterization of the assembled lipid-DNA particles. Several biophysical studies established that lipid-DNA interactions are largely defined by the electrostatic association between DNA and the cationic head groups and the high cooperativity of this association driven by hydrophobic association of the lipid tails<sup>5–7</sup>. The resulting models can reasonably well predict the energetics of lipid-DNA interactions<sup>7</sup>. This approach, however, has limitations when describing the heterogeneity of the produced lipid-DNA complexes.

Two distinct lipid-DNA complexes were identified using X-ray diffraction and optical microscopy revealed two distinct DNA-lipid complexes: (i) a multilamellar structure with

\*Corresponding author: valya@ou.edu; Phone: 1(405) 325-1677; FAX: 1(405) 325-6111.

alternating lipid bilayer and DNA monolayers and (ii) the structure, consisting of DNA coated by cationic lipid monolayers and arranged on a two-dimensional hexagonal lattice (HIIC)<sup>8,9</sup>. Both structures often co-exist in lipoplexes and their formation depends on lipid composition and formulation. As a result, lipoplexes assemble into highly heterogeneous locally ordered particles with irregular morphology<sup>10,11</sup>, whereas their structure and properties vary depending on the assembly protocol<sup>1,12,13</sup>. Thus, the folding pathway realized during lipoplex assembly is expected to define the properties of the particle.

In contrast to equilibrium studies, kinetics of lipoplex formation remains virtually unexplored. A major challenge for such studies lies in fast reaction rates and high heterogeneity of the products. Here, we investigated real-time DNA packing by cationic lipids using magnetic tweezers. In this approach, a single DNA is stretched between the surface of a capillary and a magnetic bead, and external force is applied to counteract the condensing activity of cationic lipids (Fig. 1a). As a result, the reaction can be sufficiently slowed down to resolve distinct condensation events and relate their frequencies to external conditions. This approach produced novel insights into the mechanism of DNA compaction by proteins, small polycationic molecules and detergents<sup>14–18</sup>. To extend this approach to highly heterogeneous systems, we carried out kinetic analysis of DNA condensation induced by DSTAP (1,2-stearoyl 3-triethylammonium-propane), a cationic lipid often used in DNA transfection<sup>19</sup>.

We found that DSTAP condenses DNA in a series of steps with the mean size of 60 nm. The large step size indicates that condensation is accomplished by multiple lipids and reveals the existence of hierarchy of times during lipoplex folding. The step-wise kinetics was observed both at high and low salt concentration. The times preceding the steps displayed a bimodal distribution revealing the existence of distinct condensation pathways. The fast-forming DNA-lipid complexes were more resilient to applied force. The proportion of the fast-forming, stable complexes increased at low salt concentration. Similarly, lipoplexes assembled at low salt better protected DNA from fluorescent dyes and DNase in bulk experiments. Thus, partitioning between alternative lipoplex folding pathways can be altered using external factors.

## Materials and Methods

### Lipids

5 mg DSTAP (1,2 stearoyl 3-trimethylammonium propane; Avanti Polar Lipids, Inc) was dissolved in 1 mL of 1:1 (v/v) mixture of chloroform and methanol and separated into several glass tubes. The solvent was evaporated under a dry nitrogen stream in a fume hood. The dried lipids were dissolved in sterile water (final concentration 3.6 mM) by water bath sonication until the solution clears (usually 16 min). The hydrated DSTAP was stored at 4°C for up to three months. Before experiments, the hydrated DSTAP was diluted into the reaction buffer (20 mM HEPES-KOH, pH 7.0, 0.5 mM EDTA, 0.1% Tween 20, 1 mM DTT, 75 mM NaCl) at 23°C to 200 μM, sonicated for 2 min and used within one day. If kept longer, the lipids supported gradual rather than step-wise DNA condensation (data not shown), presumably due to hydrolytic loss of one of the acyl chains.

### Magnetic tweezers

Magnetic tweezers analysis was done as previously described<sup>17</sup>. Briefly, the 8.4 kb (2.84 μm) pBB10 DNA that was stretched with high force (11 pN) between the surface of an anti-digoxigenin coated glass capillary and a streptavidin coated magnetic bead. Lipids were diluted to desired concentrations, sonicated for 30 s and introduced into the capillary. The force was then decreased to 0.5 pN and DNA extension followed in real time at 25 fps

(frames per second). Unless noted otherwise, DSTAP was used at 0.5  $\mu\text{M}$  concentration. Very few DNA condensation events could be observed at lower concentrations of the lipid. To remove the lipids from DNA for the next experiment, the capillary was rinsed with at least 15 mL of the reaction buffer containing 1 M NaCl.

Single-step analysis was done using a modification of the previous approach<sup>17</sup>. Each condensation time course was first deconvoluted into a series of trial steps using the Student's T-test. For each time point, the trial T-value was calculated within a sliding 2 s window. When T-value exceeded 1, the trial step was accepted. If T-value was greater than 1 for several consecutive points, the trial step was set in the middle of the stretch. Once the trial series was constructed, the T-value of the steps was recalculated using the complete time course. Steps with the T-value below a threshold (T equal 10) were discarded one by one beginning with the earliest time point. To this end, we were repeatedly examining all pairs of consecutive steps and eliminating steps with the smaller T-value of the two.

### DNA accessibility

Lipoplexes were prepared by mixing 500 ng of the 5.3 kb pDEV DNA (pIRES2 DsRed Express2; Clontech) with 100  $\mu\text{M}$  DSTAP at the 1:2 charge ratio in 50  $\mu\text{L}$  of the lipoplex buffer (20 mM HEPES-KOH, pH 7.0, 0.5 mM EDTA, 1 mM DTT) that was either supplemented or not with 0.25 M NaCl. Following 15 min incubation at 23°C, 7.5  $\mu\text{L}$  of the mixture was diluted into 2 mL of the lipoplex buffer containing either 0.25 M NaCl (B2) or no additional NaCl (B0) and immediately supplemented with 1 mL picogreen (1:4000 final concentration; Invitrogen). Fluorescence was measured at 525 nm (excitation at 480 nm). The percentage of DNA accessible for binding to picogreen was determined from the comparison with fluorescence from lipid-free DNA under the same conditions as previously described<sup>20</sup>.

To assess nuclease susceptibility, lipoplexes were mixed in the lipoplex buffer containing 5 mM  $\text{MgCl}_2$  and supplemented with DNase I (DN25, Sigma). Following incubation at 37 C, the reactions were quenched with 50 mM EDTA, incubated for 5 min at 23°C and analyzed by electrophoresis through 0.7% agarose gel.

## Results

### DSTAP condenses DNA in bursts

DNA condensation was monitored using the 8.4 kb (2.84  $\mu\text{m}$ ) pBB10 DNA that was stretched between the surface of a capillary and a magnetic bead (Fig. 1a). DSTAP was introduced into the capillary while DNA was kept at high force (11 pN) and then the force was reduced to 0.5 pN to initiate DNA condensation. Following a lag, DNA condensation occurred as a series of distinct steps (Fig. 1b). Increasing the force to 11 pN often recovered the initial DNA extension. However, the rate of DNA condensation markedly increased after repeated stretch-release cycles (Fig. 1b), indicating that at least some lipids remained associated with DNA even at high force. To avoid such cumulative effects, all subsequent analysis was done using data collected during the first round of DNA condensation.

The step size distribution was monomodal with the mean step increasing from  $60 \pm 5$  nm at 250 mM NaCl to  $82 \pm 7$  nm at 75 mM NaCl (Fig. 1c). This distance exceeds the size of DSTAP and, even more so, the distance between DSTAP heads within the lipid bilayer, 0.8 nm<sup>21</sup>. Thus, DNA condensation is accomplished by multiple lipids and includes a fast phase and a preceding lag. We further found that the size of the steps changes only insignificantly when DSTAP concentration is increased from 0.5  $\mu\text{M}$  ( $60 \pm 5$  nm) to 5  $\mu\text{M}$  ( $67 \pm 8$  nm) even though the overall rate of condensation increased three fold (see below). Thus each burst appears to be an independent event.

### DNA condensation is biphasic

We next quantified the time between the steps. Because the size of the steps remained roughly constant under the tested conditions, this time largely defines the rate of DNA condensation. We kept separate scores for the lag time, which is the time before condensation begins (Fig. 1b), and the rest of the pause times. In both cases, the distribution of steps was bimodal.

In about half of the cases at 250 mM NaCl, DNA condensation commenced during the first 25 s after the decrease in the stretching force (Fig. 2a). The rest of the lag times were broadly distributed and could be as high as 500 s. When analyzed as a cumulative distribution, the lag times could be fit as a double exponential decay (Fig. 2a). This view presents the lag times as a proportion of the DNA molecules that remain unreacted in the presence of the lipids. The double exponential kinetics observed in this view reveals existence of at least two distinct species of condensed DNA.

The proportion of the two species and the rates of their formation remained virtually the same at 150 mM NaCl (Fig. 2c). At 75 mM NaCl, however, the proportion of the rapidly formed complex increased to 62% and the rate of its formation increased 6-fold (Fig. 2b, c). These changes are not unexpected given that low salt conditions favor electrostatic interactions between positively charged DSTAP and negatively charged DNA. In contrast, an increase in DSTAP concentration resulted in higher condensation rates but did not affect partitioning between the fast and slow pathways (Fig. 2d). Notably, the rates of both condensation pathways remained virtually the same for 1  $\mu$ M and 5  $\mu$ M DSTAP (Fig. 2d). Thus, the rate of DNA condensation at these conditions is not limited by association of lipids with DNA.

We next performed a similar analysis of the pause times between the steps. The cumulative distributions of the pause times could, again, be fit to double exponential decays (Fig. 3). Thus, the ability to proceed via two alternative pathways remains even after the onset of DNA condensation. The rate of production of the fast-forming complex and its abundance increased with decreasing salt concentration (Fig. 3a) or an increase in concentration of DSTAP (Fig. 3b). Although not exactly the same, these trends are similar to those observed for the lag time. In particular, the distributions of the pause times were virtually the same for 150 mM and 250 mM NaCl (Fig. 3a) and for 1  $\mu$ M and 5  $\mu$ M DSTAP (Fig. 3b). In contrast to the lag times, however, the abundance of the fast-forming complex increased with the increased concentration of DSTAP (Fig. 3d). These data indicate that the first and subsequent condensation events are not entirely independent.

### Condensed DNA is a mixture of stable and unstable complexes

An increase in the force to 11 pN triggered DNA decondensation (Fig. 4a). A part of DNA length was recovered during the first second upon the increase in the force. This length often exceeded DNA slack (Fig. 4a) and was, therefore, a result of disrupted lipid-DNA interactions. The rest of DNA decondensation occurred on a slower time scale and was often incomplete during the time of experiment. Based on this distinction, we operationally defined two types of lipid-DNA complexes and quantified their abundance as illustrated in Fig. 4a.

The partitioning between the stable and unstable complexes displayed a marked dependence on salt concentration (Fig. 4b). The proportion of the stable complex increased from 16% at 250 mM NaCl to 73% at 75 mM NaCl. Similar distributions were obtained when we used a smaller, 7 pN force for DNA decondensation (Fig. 4b, c). This result points to a significant energetic gap between the two complexes and suggests that they have different structures.

### Abundance of stable lipoplexes can be varied in bulk

We next tried to recuperate the observed partitioning between alternative folding pathways in bulk experiments. To this end, we prepared lipoplexes at high (250 mM NaCl) and low (0 mM NaCl) salt concentration and then determined if the choice of the assembly protocol has any effect on DNA accessibility. In brief, lipoplexes were diluted into solutions of DNA sensitive fluorescent dye picogreen, and the resulting fluorescence was compared to that in the presence of lipid-free DNA. The ratio of the two was used as a measure of picogreen-accessible DNA.

We found little difference between the two types of lipoplexes when the dilution was done into the low salt solution. Within few minutes, picogreen fluorescence reached its plateau at, approximately, 20% accessible DNA (Fig. 5a). A similarly fast kinetics was observed when lipoplexes were prepared at high salt and then diluted into the high salt solution. For this salt concentration, the saturation level of picogreen binding was at 90% (Fig. 5a). In all these cases, the binding of picogreen could be modeled as a single-exponential kinetics with characteristic rates in the sub-minute range (Fig. 5c). In contrast, the binding of picogreen to the low-salt lipoplexes diluted into 250 mM NaCl displayed biphasic kinetics (Fig. 5a, c). Only half of the observed fluorescence increase happened during the first minute of experiment, whereas the rest of lipoplex unfolding occurred on a 100-fold slower time scale. The results were virtually the same if lipoplex unfolding was done in the presence of magnesium (Fig. 5b, d), which further argues for the existence of stable and unstable phases within the lipoplex.

The stable lipid-DNA complexes were more resilient to nuclease degradation. For lipoplexes prepared at low salt conditions, about 3-fold more DNase I was needed to achieve the same DNA cleavage as for naked DNA. In contrast, the high salt lipoplexes were only 50% more resilient to DNase I (Fig. 5e). A similar result was obtained when lipoplexes were treated with constant amount of DNase I for various times (Fig. 5f). At these conditions, the disappearance of uncut DNA was bimodal, with the life-time of uncut DNA increasing from 0.7 min for naked DNA to 22 min for the low salt lipoplexes. Thus, lipoplex folding in bulk also proceeds via two alternative pathways and the partitioning between the two pathways can be altered by salt concentration.

### Discussion

Using magnetic tweezers, we followed assembly of lipoplexes in real time. The reaction involved DNA condensation and occurred as a series of steps. Most of the steps were bigger than the DSTAP molecule (Fig 1c) and, therefore, resulted from DNA interaction with multiple lipids. Such kinetics bears resemblance to the previously studied cases of DNA condensation. In the presence of cationic dendrimers and detergents, DNA condensation began after a lag and continued with a steady rate<sup>16, 18</sup>. A similar pattern was observed for condensins, DNA binding proteins involved in chromosome maintenance<sup>15, 17</sup>. Such behavior is consistent with the nucleation-propagation mechanism where nucleation limits the overall rate of the reaction. When applied to condensin-induced DNA condensation, this model could quantitatively predict the relationship between the lag time and the condensation rate<sup>17</sup>. The lag-burst kinetics observed for DSTAP is consistent with the nucleation-propagation mechanism.

In contrast to the other cases, DSTAP-mediated DNA condensation was interrupted by numerous long pauses. The length of the pauses was comparable to the lag time, indicating that each condensation step is a separate event. Such kinetics sets DSTAP apart from other studied condensing agents and might be attributable to the ability of double-tail lipids to form bilayers. This idea is tentatively supported by the finding that after long storage,

DSTAP solutions induced gradual rather than step-wise DNA condensation (data not shown). Such gradual condensation has been reported for cationic detergents<sup>18</sup> and would be expected upon hydrolytic conversion of DSTAP into monostearoyl trimethylammonium propane.

The observed step-wise kinetics could be explained by postulating that each step arises due to DNA packing by a single lipid vesicle. In this view, the pause time is defined by the frequency of random collisions between the vesicles and DNA. This view, however, is at odds with the finding of step-wise kinetics at saturating concentrations of DSTAP (Fig. 3b, d). Apparently the rate limiting step in this reaction occurs after lipids associate with DNA. A plausible candidate here would be some sort of structural rearrangement in the complex between DNA and the lipid bilayer that deforms the DNA and creates a stable nucleus. The size of the steps would then reflect the size of the resulting folded lipoplex domains. Because the mean step size increased at the lower salt concentration (Fig. 1), one is tempted to conclude that the size of the lipoplex domains depends not only on the size of the lipids but also on the energetics of lipid-DNA interactions. Investigation of the force-dependence of condensation steps and lipoplex stability should provide additional insights into the structure of these domains.

Curiously, the rate of DNA condensation was not affected by lipid concentration above 1  $\mu\text{M}$  DSTAP. The distributions of both the lag and pause times were virtually identical for 1  $\mu\text{M}$  and 5  $\mu\text{M}$  DSTAP (Figs. 2d, 3b). Such saturation could occur if the entire DNA was coated by the lipids at these levels of DSTAP. Alternatively, the molecule could be associated with only a few lipid vesicles. Being bulky and highly charged, the vesicles could limit further binding due to steric or electrostatic repulsion.

Kinetic analysis of the lag (Fig. 2) and pause (Fig. 3) times preceding the steps revealed two distinct types of condensation events. Some of the steps followed each other in rapid ( $\sim 10$  s) succession whereas others were separated by several minutes. When analyzed as a cumulative distribution, the pause times could be approximated as a double exponential decay. Such kinetics occurs when a reaction is controlled by two slow steps. In principle, these slow steps could occur either consecutively or in parallel to each other.

The two possibilities can be distinguished by analyzing stability of the lipoplexes. The former case envisions a single DNA condensation pathway with no apparent relationship between stability of the product and the rate of its formation. If anything, the slower produced complex should be more stable. In the latter case, the two parallel reactions are expected to produce two distinct complexes that would behave differently during decondensation. This is exactly the pattern that was observed in experiment. Two distinct species of lipid-DNA complexes could be recognized based on their ability to withstand elevated force, and the abundance of the stable species increased under conditions that favored fast DNA condensation (Fig. 4c). We conclude, therefore, that lipoplex formation proceeds via two parallel pathways, with the fast forming complex being also more resilient to applied force.

Notably, the existence of two lipid-DNA complexes was confirmed in bulk experiments. Lipoplexes assembled at low salt conditions more efficiently protected DNA from nuclease (Fig 5e, f) and fluorescent dyes (Fig. 5a, b) than the high salt lipoplexes. This result mirrors the finding from DNA stretching experiments that low salt conditions favor production of stable DSTAP-DNA complexes (Fig 4). This agreement lays ground for potential use of single molecule methods in lipoplex design. Exploration of the DNA condensation pathways as a function of lipid structure and composition could conceivably help design lipoplexes with desired properties.

Our finding that lipoplex folding occurs via two parallel pathways highlights the importance of heterogeneity in defining the properties of matter even at the single molecule level. Finding ways to characterize and control such heterogeneity might be critical for nanoscale engineering.

## Conclusions

Cationic lipids induce DNA condensation, which can be monitored using magnetic tweezers.

Lipid-induced DNA condensation occurs as a series of distinct steps with the mean step size bigger than the size of the lipid. Such kinetics is consistent with the nucleation- propagation mechanism of DNA condensation. The step size increases with decreasing salt concentration, which reveals the role of electrostatics in defining cooperativity of the process.

The distribution of pause times between the steps is bimodal, which points to two separate DNA condensation pathways. The proportion of the fast forming complex increases at lower salt concentration.

Force induced decondensation of lipoplexes is biphasic. The proportion of the stable complex correlates with the fraction of DNA that was rapidly condensed during formation of the lipoplexes. Thus, lipoplexes are structurally heterogeneous with the faster produced phase being more stable.

The existence of the two complexes can be reproduced in bulk experiments. The more stable complex is also better in protecting DNA from fluorescence dyes and nuclease degradation. Similar to single molecule experiments, the stability of the lipoplexes increases at low salt concentration. Thus, single molecule studies can be used for optimization of lipoplexes.

## Acknowledgments

This work was supported by a grant EB009238 to VVR from the National Institutes of Health.

## References

1. Li W, Szoka FC Jr. Lipid-based Nanoparticles for Nucleic Acid Delivery. *Pharm Res.* 2007
2. Patil SD, Rhodes DG, Burgess DJ. DNA-based therapeutics and DNA delivery systems: a comprehensive review. *Aaps J.* 2005; 7(1):E61–77. [PubMed: 16146351]
3. Simoes S, Filipe A, Faneca H, Mano M, Penacho N, Duzgunes N, de Lima MP. Cationic liposomes for gene delivery. *Expert Opin Drug Deliv.* 2005; 2(2):237–54. [PubMed: 16296751]
4. Zuhorn IS, Hoekstra D. On the mechanism of cationic amphiphile-mediated transfection. To fuse or not to fuse: is that the question? *J Membr Biol.* 2002; 189(3):167–79. [PubMed: 12395282]
5. Mel'nikova YS, Mel'nikov SM, Lofroth JE. Physico-chemical aspects of the interaction between DNA and oppositely charged mixed liposomes. *Biophys Chem.* 1999; 81(2):125–41. [PubMed: 17030332]
6. Rosa H, Petri DF, Carmona-Ribeiro AM. Interactions between bacteriophage DNA and cationic biomimetic particles. *J Phys Chem B.* 2008; 112(51):16422–30. [PubMed: 19367939]
7. Matulis D, Rouzina I, Bloomfield VA. Thermodynamics of cationic lipid binding to DNA and DNA condensation: roles of electrostatics and hydrophobicity. *J Am Chem Soc.* 2002; 124(25):7331–42. [PubMed: 12071742]
8. Koltover I, Salditt T, Radler JO, Safinya CR. An inverted hexagonal phase of cationic liposome-DNA complexes related to DNA release and delivery. *Science.* 1998; 281(5373):78–81. [PubMed: 9651248]

9. Radler JO, Koltover I, Salditt T, Safinya CR. Structure of DNA-Cationic Liposome Complexes: DNA Intercalation in Multilamellar Membranes in Distinct Interhelical Packing Regimes. *Science*. 1997; 275(5301):810–814. [PubMed: 9012343]
10. Braun CS, Jas GS, Choosakoonkriang S, Koe GS, Smith JG, Middaugh CR. The structure of DNA within cationic lipid/DNA complexes. *Biophys J*. 2003; 84(2 Pt 1):1114–23. [PubMed: 12547792]
11. Prasad TK, Gopal V, Rao NM. Cationic lipids and cationic ligands induce DNA helix denaturation: detection of single stranded regions by KMnO<sub>4</sub> probing. *FEBS Lett*. 2003; 552(2–3): 199–206. [PubMed: 14527687]
12. Gao X, Huang L. Potentiation of cationic liposome-mediated gene delivery by polycations. *Biochemistry*. 1996; 35(3):1027–36. [PubMed: 8547238]
13. Wheeler JJ, Palmer L, Ossanlou M, MacLachlan I, Graham RW, Zhang YP, Hope MJ, Scherrer P, Cullis PR. Stabilized plasmid-lipid particles: construction and characterization. *Gene therapy*. 1999; 6(2):271–81. [PubMed: 10435112]
14. Baumann CG, Bloomfield VA, Smith SB, Bustamante C, Wang MD, Block SM. Stretching of single collapsed DNA molecules. *Biophys J*. 2000; 78(4):1965–78. [PubMed: 10733975]
15. Strick TR, Kawaguchi T, Hirano T. Real-time detection of single-molecule DNA compaction by condensin I. *Curr Biol*. 2004; 14(10):874–80. [PubMed: 15186743]
16. Ritort F, Mihardja S, Smith SB, Bustamante C. Condensation transition in DNA-polyaminoamide dendrimer fibers studied using optical tweezers. *Phys Rev Lett*. 2006; 96(11):118301. [PubMed: 16605879]
17. Cui Y, Petrushenko ZM, Rybenkov VV. MukB acts as a macromolecular clamp in DNA condensation. *Nat Struct Mol Biol*. 2008; 15(4):411–8. [PubMed: 18376412]
18. Husale S, Grange W, Karle M, Burgi S, Hegner M. Interaction of cationic surfactants with DNA: a single-molecule study. *Nucleic Acids Res*. 2008; 36(5):1443–9. [PubMed: 18203749]
19. Filion MC, Phillips NC. Toxicity and immunomodulatory activity of liposomal vectors formulated with cationic lipids toward immune effector cells. *Biochimica et biophysica acta*. 1997; 1329(2): 345–56. [PubMed: 9371426]
20. Bunuales M, Duzgunes N, Zalba S, Garrido MJ, de Ilarduya CT. Efficient gene delivery by EGF-lipoplexes in vitro and in vivo. *Nanomedicine (Lond)*. 2011; 6(1):89–98. [PubMed: 21182421]
21. Nagle JF, Tristram-Nagle S. Structure of lipid bilayers. *Biochimica et biophysica acta*. 2000; 1469(3):159–95. [PubMed: 11063882]

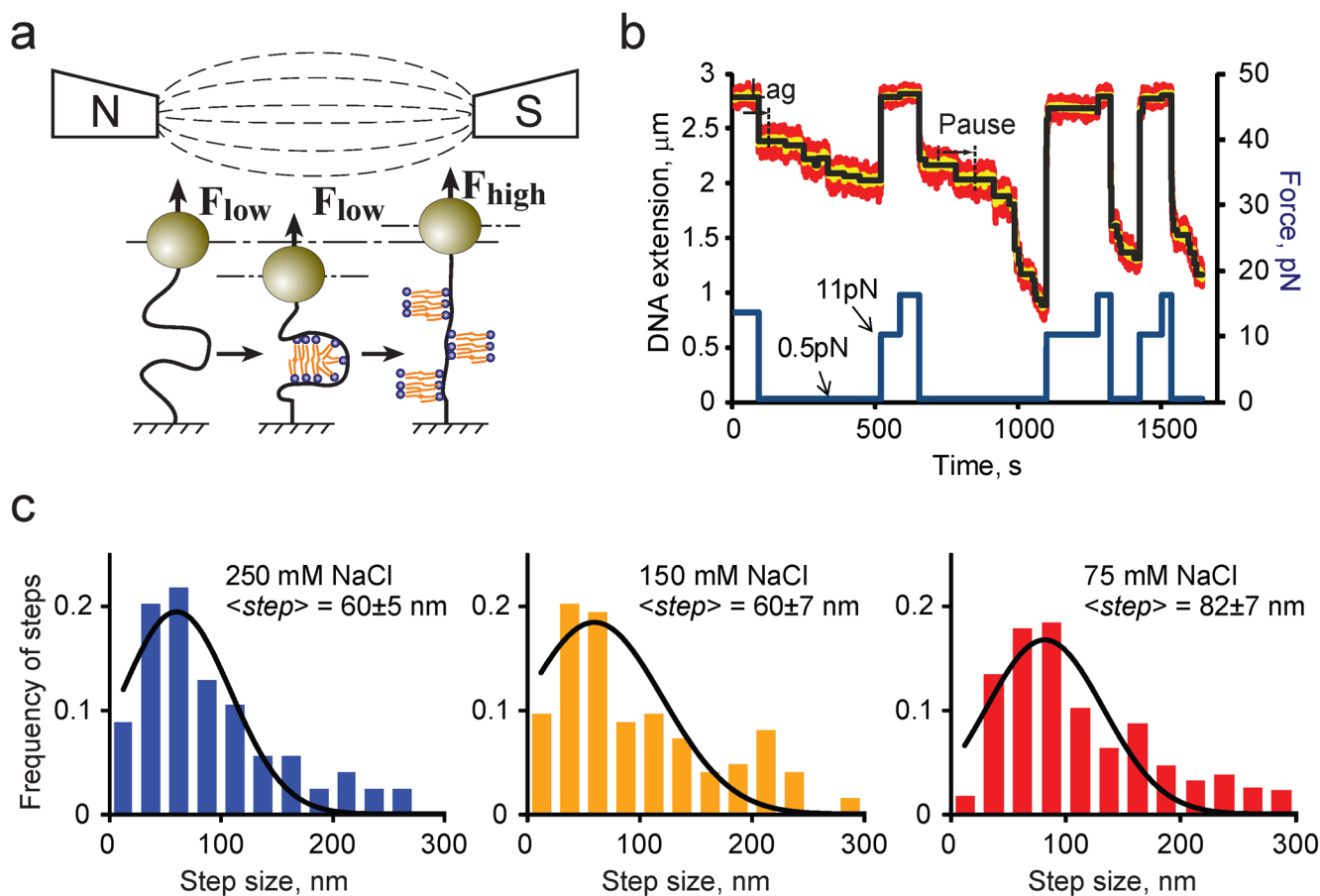


**Figure 1. Condensation of a single DNA by DSTAP**

(a) Real time analysis of DNA condensation using magnetic tweezers. The force is applied from a pair of magnets placed above the capillary, and DNA extension is followed in real time using videomicroscopy.

(b) DNA condensation and decondensation during multiple stretch-release rounds. DNA condensation is initiated by the reduction in force to 0.5 pN and, after a lag, proceeds as a series of steps separated by pauses. At high force, DNA decondenses. Shown are the real time DNA extensions (red), the real time data filtered at 1 Hz (yellow) and step-wise approximation of DNA condensation (black).

(c) Distribution of step sizes found at the indicated NaCl concentrations. The data were fit to a Gaussian distribution (black), and the mean step sizes ( $\pm$  SEM) are shown on the plots.

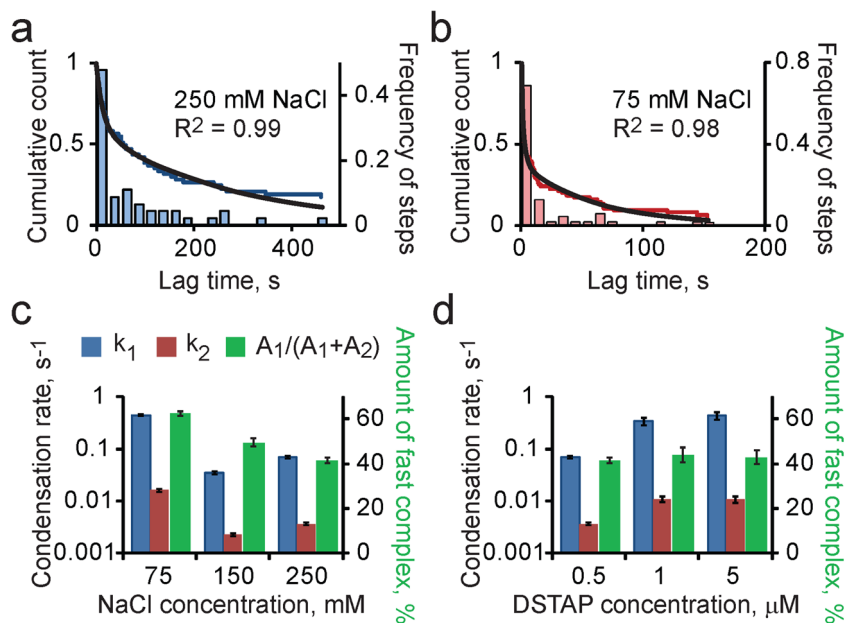


**Figure 2. Kinetic analysis of the lag times preceding DNA condensation**

(a, b) The lag time distributions for 250 mM (a) and 75 mM (b) NaCl. The lag times were binned according to their length and plotted as differential (bars, right axes) or cumulative (lines, left axes) distributions. The cumulative distributions were then approximated as double-exponential decays (black lines). The goodness-of-fit  $R^2$  values ( $n > 56$ ) are indicated on each plot.

(c, d) The best fit rate constants and amplitudes for cumulative lag time distributions plotted against concentration of NaCl (c) or DSTAP (d). The error bars show the fitting errors.

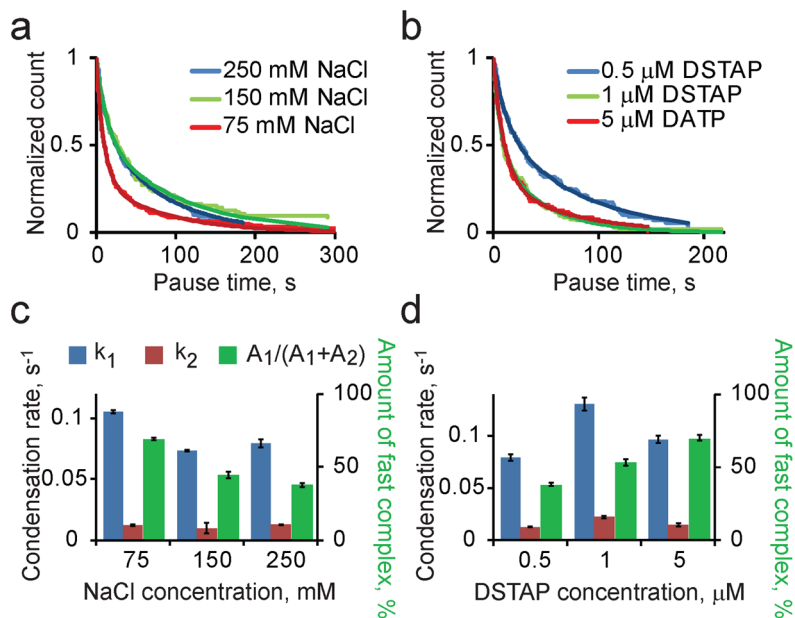


**Figure 3. Kinetic analysis of the delay times between condensation steps**

(a, b) Cumulative distributions of the delay times observed at various concentrations of NaCl (a) or DSTAP (b). The distributions were fit to double exponential decays (all  $R^2$  values greater than 0.99).

(c, d) The best fit rate constants and amplitudes for cumulative distributions of delay times plotted against concentration of NaCl (c) or DSTAP (d). The error bars show the fitting errors.

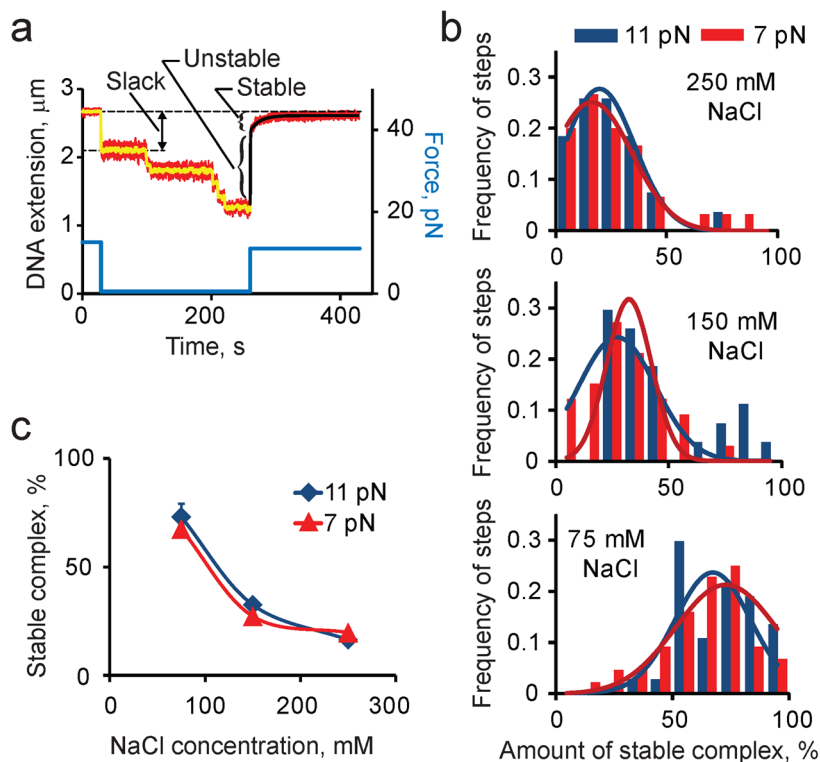


**Figure 4. Analysis of the force-induced decondensation of lipoplexes**

(a) Decondensation of lipoplexes includes the fast and slow phases. The time course of decondensation was fitted to a double exponential decay function (solid black line), and the amount of the unstable complex determined as the amplitude of the fast exponent. The rest of the condensed DNA was defined as the stable complex.

(b) The frequency of finding the indicated proportion of condensed DNA found in the stable complex at various NaCl concentrations and stretching forces ( $n > 27$ ). The data were fit to Gaussian distributions (black lines).

(c) The amount of condensed DNA in the stable complex (mean  $\pm$  SEM) as a function of NaCl concentration.

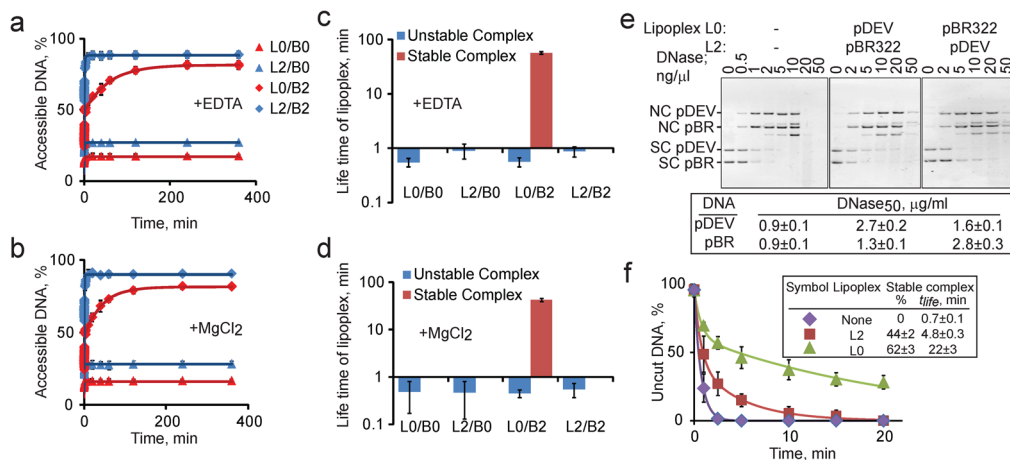


**Figure 5. DNA accessibility in lipoplexes prepared at high and low NaCl concentrations**

(a, b) Time course of picogreen binding to DNA in lipoplexes prepared at 250 mM (L2) or 0 mM (L0) NaCl upon their dilution into the buffer containing 250 mM (B2) or 0 mM (B0) NaCl and either 1 mM EDTA (a) or 5 mM  $\text{MgCl}_2$  (b). The amount of picogreen bound DNA was determined from the comparison of picogreen fluorescence with that in the presence of lipid-free DNA. The data were analyzed as a single exponential or, for the L0 lipoplex diluted in the B2 buffer (L0/B2), a double exponential decay (black lines). The error bar indicates SD ( $n = 3$ ).

(c, d) Life times of the stable and unstable complexes detected using the picogreen binding assay in panels a and b.

(e) DNase sensitivity of lipoplexes assembled at high (L2) and low (L0) salt conditions. A mixture of 30 ng supercoiled pDEV and pBR322 DNA or lipoplexes containing the same DNAs was treated with the indicated amounts of DNase I for 5 min in 20  $\mu\text{L}$  of lipoplex buffer, quenched with 2  $\mu\text{L}$  of 500 mM EDTA and analyzed by gel electrophoresis. The reactions contained naked DNA (left), a mixture of the low salt pDEV and the high salt pBR322 lipoplexes (middle), or the mixture of the low salt pBR322 and the high salt pDEV lipoplexes (right). The amount of uncut DNA was quantified as a single exponential decay, and the best fit amount of DNase needed to cut 50% DNA is shown below the gels.

(f) Time course of DNA degradation ( $\pm$  SD;  $n=3$ ) during treatment with 16 ng DNase I. The data were fitted as a single- (naked DNA) or double- (lipoplexes) exponential decay. The amplitude and life time of the slow-decaying exponent is shown on the graph. The life-time of the naked DNA and the unstable lipoplex was  $0.7\pm 0.1$  min.